MicroRNA Expression Patterns Involved in Amyloid Beta–Induced Retinal Degeneration

Peirong Huang,[1,2] Junran Sun,[1,2] Fenghua Wang,[1,2] Xueting Luo,[3] Jingyang Feng,[1,2] Qing Gu,[2] Te Liu,[4] and Xiaodong Sun[1–3]

[1]Department of Ophthalmology, Shanghai First People's Hospital, Shanghai Jiao Tong University School of Medicine, Shanghai, People's Republic of China
[2]Shanghai Engineering Center for Visual Science and Photomedicine, Shanghai, China
[3]Shanghai Key Laboratory of Fundus Diseases, Shanghai, People's Republic of China
[4]Shanghai Geriatric Institute of Chinese Medicine, Longhua Hospital, Shanghai University of Traditional Chinese Medicine, Shanghai, People's Republic of China

Correspondence: Xiaodong Sun, Department of Ophthalmology, Shanghai First People's Hospital, Shanghai Jiao Tong University School of Medicine, Shanghai Key Laboratory of Fundus Diseases, Shanghai Engineering Center for Visual Science and Photomedicine, 100 Hai Ning Road, Shanghai 200080, People's Republic of China; xdsun@sjtu.edu.cn.
Te Liu, Shanghai Geriatric Institute of Chinese Medicine, Longhua Hospital, Shanghai University of Traditional Chinese Medicine, Building C, 365 Xiangyang Road, Shanghai 200031, People's Republic of China; liute1979@126.com.

PH and JS contributed equally to the work presented here and should therefore be regarded as equivalent authors.

Submitted: June 9, 2016
Accepted: February 16, 2017

Citation: Huang P, Sun J, Wang F, et al. MicroRNA expression patterns involved in amyloid beta–induced retinal degeneration. *Invest Ophthalmol Vis Sci*. 2017;58:1726–1735. DOI: 10.1167/iovs.16-20043

Purpose. Dry age-related macular degeneration (AMD) is characterized by the accumulation of drusen under Bruch's membrane, and amyloid beta (Aβ) is speculated to be one of the key pathologic factors. While the detrimental effects of Aβ on retinas have been widely explored, Aβ-induced epigenetic regulatory changes have yet to be fully investigated. We therefore aimed to identify the microRNA (miRNA) expression profiles in an Aβ-induced mouse model of retinal degeneration.

Methods. C57BL/6 mice were intravitreally injected with $A\beta_{1\text{-}40}$ or PBS and the eye tissues were collected for hematoxylin and eosin (H&E) staining, apoptosis immunofluorescence staining, and miRNA profiling. After filtering, 10 miRNAs and their target genes were chosen for quantitative RT-PCR (qRT-PCR) confirmations. Pathway analyses were employed for further bioinformatic analyses.

Results. Hematoxylin and eosin–stained sections of retinal pigment epithelium (RPE)/neural retina tissue demonstrated degenerative alterations, and immunofluorescence testing revealed apoptosis within the retina after Aβ treatments. MicroRNA profiling revealed 61 miRNAs that were differentially expressed between the model and the control group. Among these, 38 miRNAs were upregulated (fold change > 1.5, $P < 0.05$) and 23 miRNAs were downregulated (fold change < 0.667, $P < 0.05$). Five of the 10 selected miRNAs (miR-142, miR-216, miR-155, miR-223, and miR-433) as well as several key target genes (*CFH*, *IGF-1R*, *c-MET*, and *ABCA1*) were confirmed by qRT-PCR analyses.

Conclusions. Our study is the first to profile the miRNA expression patterns and suggests that Aβ accumulation could lead to relevant biochemical alternations such as complement activation, barrier impairment, apoptosis, and positive feedback of Aβ production.

Keywords: amyloid beta, retina, microRNA, age-related macular degeneration

Age-related macular degeneration (AMD) is the leading cause of untreatable blindness in Western countries.[1,2] Anti-VEGF therapy has been greatly effective for the wet/neovascular form of AMD; however, no effective therapies are available for the dry/atrophic form.[3] Dry AMD is characterized by the accumulation of drusen under Bruch's membrane,[4] and amyloid beta (Aβ) is a main component of these drusen.[5] Amyloid beta metabolic dysregulation is also hypothesized to contribute to Alzheimer's disease (AD). Interestingly, several transgenic mouse models overexpressing Aβ, such as 5XFAD and *neprilysin*$^{-/-}$ mice, develop retinal pigment epithelial (RPE) degeneration and basal deposits similar to dry AMD patients.[6,7] In addition, several studies have reported on the potential of anti-Aβ therapeutic strategies and their impact on functional recovery in experimental AMD rat models, implying the vital role of Aβ in the retina.[8,9]

Recently, intravitreally injected $A\beta_{1\text{-}40}$, instead of the more AD-specific $A\beta_{1\text{-}42}$ peptide, has been used to produce an in vivo model of Aβ stimulation on the retina.[10] $A\beta_{1\text{-}40}$ is the principal form found in the ocular fluids[11] and drusen.[5] The gene expression profile in response to $A\beta_{1\text{-}40}$ stimulation in hRPE cells has been reported.[12] After intravitreal Aβ injection, Aβ was found across all neuropil and extracellular compartments of the neuroretina layers, as indicated by diffuse staining with the Aβ-specific antibody 4G8.[13] Positive Aβ staining was also observed in the RPE as discrete intracellular vesicles because the RPE continuously phagocytoses the outer segment discs.[13] This model could partially simulate how Aβ disturbs the normal

physiological processes and influences the morphologic appearance of the retina and RPE/choroid in AMD eyes.

Studies have demonstrated the detrimental roles of Aβ on the structure, homeostasis, properties, and functions of the retina. It has been made clear that Aβ can accelerate cell stress and the aging process, vital pathologic processes in AMD initiation and progression.[14,15] Furthermore, elevated Aβ deposits can induce a proinflammatory microenvironment and subsequently activate the complement system.[10,16] Interestingly, Aβ can also induce the upregulation of angiogenic factors as well as break down the outer barrier of retinas, which might play a role in subtype conversion.[17,18] However, the epigenetic changes caused by Aβ have not been fully investigated.

MicroRNAs (miRNAs) have emerged as a new therapeutic direction for several diseases,[19] including neurodegenerative disorders.[20] MicroRNAs are single-stranded short (21–23 nucleotides long) noncoding RNAs that are involved in posttranscriptional modulation. Each miRNA can specifically inhibit its target mRNA's function by binding to the complementary site.[21] MicroRNAs are crucial in normal biological development and metabolism. In disease states, their expression levels change. Balancing the level of miRNAs is a new area of therapeutic targeting.[20] Furthermore, the miRNA metabolism in neurons, such as photoreceptors, is higher than in other cell types.[22] Prior studies showed differential levels of secreted miRNAs (miR-301-3p, -361-5p, and -424-5p) in wet AMD patients,[23] and neurovascularization could be repressed by certain miRNA targets, including microRNA-24.[24] Kaneko et al.[25] found that miRNA processing of the enzyme DICER1 was reduced in the RPE of humans with geographic atrophy (GA) and that conditional *DICER1* ablation induced RPE degeneration. However, studies on the role of miRNA regulation in Aβ stimulation in the retina are limited.

MicroRNA microarrays facilitate the analysis of miRNA expression patterns and quantification of the levels in a high-throughput screening manner.[26] We therefore aimed to profile the miRNA expression changes in Aβ-induced retinal degeneration using microarray chips, information that has not been previously reported. The observations of our study may provide clues for the pathologic regulation of miRNAs in the $A\beta_{1\text{-}40}$-induced retina degeneration model and provide potential interventional targets for further research.

Materials and Methods

Amyloid Preparation

$A\beta_{1\text{-}40}$ (GL Biochemistry, Shanghai, China) was prepared as previously described.[27] Briefly, Aβ peptides were dissolved in double-distilled H_2O at a concentration of 28 μg/μL and then immediately added to phosphate-buffered saline (PBS) to obtain a final concentration of 2.8 μg/μL. The mixture was incubated at 37°C for 7 days prior to use. The aggregated states were checked by electron microscopy.

Animal Model and Treatment

Two-month-old male C57BL/6 mice were supplied by the Laboratory Animal Center at the Shanghai First People's Hospital, raised on a standard rodent diet, and housed with a 12-hour light/dark cycle. The experiments strictly conformed to the ARVO Statement for the Use of Animals in Ophthalmic and Vision Research. All animal experiments were approved by the Ethics Committee of Jiao Tong University, Shanghai, China.

To explore the Aβ-induced miRNA expression profile, six mice were anesthetized with 1.5% sodium pentobarbital (100 μL/20 g intraperitonally) and underwent a single unilateral intravitreal injection (IVL) with $A\beta_{1\text{-}40}$ peptides (14 μg/5 μL) in PBS, which is comparable to other in vivo studies.[10] Briefly, the IVL was administered under a dissecting microscope (stereo dissection microscope, SMZ 1000; Nikon, Tokyo, Japan) using a 32-gauge Hamilton needle and syringe (Hamilton, Reno, NV, USA) to deliver 5 μL oligomeric $A\beta_{1\text{-}40}$ peptides. Six age-matched controls received 5 μL PBS in the same manner. The mice were kept for 48 hours, and then their eyes were enucleated and preserved in 4% paraformaldehyde in Dulbecco's PBS (DPBS; Invitrogen, Carlsbad, CA, USA) under intraperitoneal anesthesia.

Hematoxylin and Eosin (H&E) Staining

Tissue sections were embedded in paraffin and then cut to a thickness of 4 μm as previously described.[28,29] Sections from within 200 μm of the optic disc were chosen for processing because they were assumed to have a similar thickness.[30] Briefly, after deparaffinization and rehydration, sections were treated with sodium citrate buffer (pH 6.0, 10 minutes) and blocking buffer (10% normal goat serum, 0.05% Triton X-100 in PBS; 1 hour, room temperature). Then, the specimens were stained with H&E. The slides were dehydrated and placed on a coverslip.

Annexin V-FITC/PI Assay

Enucleated eyes were immediately fixed with 10% formalin and embedded in paraffin. Apoptosis was evaluated using an Annexin V-FITC kit (Beyotime Institute of Biotechnology, Haimen, Jiangsu, China) according to the manufacturer's protocols. Annexin V-FITC was used to reveal the level of apoptosis using a fluorescence microscope. The sections were stained with propidium iodide (PI) (1:3000; Molecular Probes, Eugene, OR, USA) for 30 minutes to determine the retinal cell distribution.

Total RNA Extraction

Total RNA extraction and quantification were performed as previously described.[31] Briefly, total RNA was extracted from tissue using the TRIzol reagent (Invitrogen Life Technologies, Carlsbad, CA, USA). The RNA samples were treated with DNase I (Sigma-Aldrich Corp., St. Louis, MO, USA) and then quantified on a NanoDrop 2000c spectrophotometer (Thermo Fisher Scientific, Wilmington, DE, USA).

miRNA Microarray and Analysis

Neuroretina and RPE/choroid tissues were all collected from multiple eyes for total RNA extraction. RNA labeling and hybridization were performed using a miRNA microarray chip from KangChen Bio-Tech (Shanghai, China) following the manufacturer's protocol. Briefly, the total RNA samples from both the Aβ-injected and vehicle groups were labeled using a miRCURY HY3 Power labeling kit (Exiqon, Vedbæk, Denmark). Hybridization was performed on a miRCURY LNA Array Manual (Exiqon). Finally, images of the microarray were scanned on an array scanner (Axon GenePix 4000B; Molecular Devices, Sunnyvale, CA, USA) and the signal intensity values were quantified.

The results were subsequently analyzed using GenePix Pro 6.0 software (Axon Instruments, Sunnyvale, CA, USA). Volcano plot filtering was employed to identify the significantly differentially expressed miRNAs between the control and treatment groups. The thresholds we used to identify up- or

Investigative Ophthalmology & Visual Science

Table 1. MiRNA qRT-PCR Primers Used in the Study

Accession No.	miRNA	qRT-PCR Primers (5′→3′) *Forward
MIMAT0000155	mmu-miR-142a-3p	tgtagtgtttcctactttatgga
MIMAT0009456	mmu-miR-1839-5p	aaggtagatagaacaggtcttg
MIMAT0003729	mmu-miR-216b-5p	aaatctctgcaggcaaatgtga
MIMAT0000165	mmu-miR-155-5p	ttaatgctaattgtgatagggggt
MIMAT0000665	mmu-miR-223-3p	tgtcagtttgtcaaatacccca
MIMAT0004187	mmu-miR-744-5p	tgcggggctagggctaacagca
MIMAT0001420	mmu-miR-433-3p	atcatgatgggctcctcggtgt
MIMAT0005460	mmu-miR-1224-5p	gtgaggactggggaggtggag
MIMAT0000233	mmu-miR-200b-3p	taatactgcctggtaatgatga
MIMAT0000376	mmu-miR-298-5p	ggcagaggagggctgttcttccc
MIMAT0000667	mmu-miR-33-5p	gtgcattgtagttgcattgca
MIMAT0000158	mmu-miR-146a-5p	tgagaactgaattccatgggtt

* Reverse transcription primer: 5′-GCTGTCAACGATACGCTACCTA-3′, according to the cDNA synthesis kit.

downregulated miRNAs were fold change greater than 1.5 and *P* value less than 0.05.

Quantitative Real-Time PCR (qRT-PCR) Validation of miRNA Expression

MicroRNAs were chosen for further qRT-PCR analysis based on the following criteria: an up- or downregulated fold change greater than 1.5 as screened by the microarray; miRNA star forms were excluded; and the top five up- or downregulated miRNAs were chosen after filtering. Total RNA was isolated using the miRcute miRNA Isolation Kit (Tiangen, Beijing, China). The poly(A) tail was added to the 3′-terminal of the miRNA, and the first-strand cDNA was synthesized using a miRcute miRNA First-strand cDNA Synthesis Kit (Tiangen). The target cDNA was amplified using a miRcute miRNA qPCR Detection Kit (SYBR Green, Tiangen) according to the manufacturer's protocol. The primers used for the 18S sequence were 5′-AGGGGAGAGCGGGTAAGAGA-3′ (forward) and 5′-GGACAGGACTAGGCGGAACA-3′ (reverse).

The RT-PCR reactions for 18S and the 10 miRNAs were performed using a real-time PCR detection system (Eppendorf, Hamburg, Germany) with 40 PCR cycles (denaturation at 95°C and then annealing at 57°C for 10 seconds). SYBR Green RealTime PCR Master Mix (Toyobo, Osaka, Japan) was used to demonstrate any change in the fluorescence intensity. The relative expression for each miRNA was calculated using the expression $2^{-\Delta\Delta Ct}$ method. The miRNA primers used are listed in Table 1.

Biologic Functional Analyses

All of the miRNAs confirmed by PCR were included in the biologic functional analyses. We used three databases—miRBase (http://www.mirbase.org/, in the public domain), miRanda (http://www.microrna.org/, in the public domain), and TargetScan (http://www.targetscan.org/, in the public domain) to specify the potential miRNA target genes. The targets were then subjected to functional analysis via Kyoto Encyclopedia Genes and Genomes (KEGG) pathways. A *P* value less than 0.05 was considered to be statistically significant.

Quantitative Real-Time PCR Validation of mRNA Expression

Quantitative RT-PCR was conducted according to our former published studies.[32] Briefly, the first-strand cDNA was synthesized from 2 μg total RNA in a 20-μg mixture according to the protocol for the RT Master Mix (Takara Bio, Inc., Dalian, China). Glyceraldehyde-3-phosphate dehydrogenase (GAPDH) was used to normalize all of the samples. Respectively, the specific sense and antisense primer sequences used were as follows: *CFH*, 5′-CTCGCTGTGTTGGACTTCCTT-3′ and 5′-GTATGTAACCTCTTCCCCATGTTG-3′; *ABCA1*, 5′-CAGAAGG GAGTGTCAGAAAT-3′ and 5′-GAAACAGCCCAGTCAGTATT-3′; *c-MET*, 5′-ACCTCAGCAATGTCAGCACCA-3′ and 5′-GGCCATGT GATGTCATTCTGG-3′, *IGF-1R*, 5′-GGAGGAGTTCGAGACAGA GTA-3′ and 5′-CGATGCGGTACAGAGTGAAA-3′; and *GAPDH*, 5′-AGGCCGGTGCTGAGTATGTC-3′ and 5′-TGCCTGCTTCAC CACCTTCT-3′. The RT-PCR reactions were performed using a real-time PCR detection system (Eppendorf; 40 cycles of 95°C for 15 seconds, 58°C for 30 seconds, and 60°C for 45 seconds). The SYBR Green RealTime PCR Master mix (Toyobo) was used to demonstrate any change in the fluorescence intensity. The relative expression for each mRNA was calculated using the expression $2^{-\Delta\Delta Ct}$ method.

Statistical Analysis

Each experiment was performed in triplicate, and the data are expressed as the mean ± SEM, where applicable. The statistical significance of differences was evaluated using Student's *t*-test. A *P* value less than 0.05 was considered statistically significant.

Results

Aβ-Induced Retinal Degeneration and Mild Apoptosis in the Outer Retina

To investigate the pathologic effects of $A\beta_{1\text{-}40}$ on the retina, H&E-stained sections of RPE/neural retinal tissue were examined (Fig. 1). The PBS-injected group showed normal-appearing retinas (Fig. 1A), while the Aβ-injected mice showed retinal degenerative changes (Fig. 1B). These alterations included hyperpigmentation (red triangles), hypopigmentation (white arrows), and obvious disorganization of the outer nuclear layer (ONL) (Fig. 1D).

We further explored the effect of $A\beta_{1\text{-}40}$ on retinal apoptosis. Immunofluorescence assays revealed double-positive staining (Annexin V^+ and PI^+) in the inner nuclear layer (INL) and ONL (Fig. 2). Apoptosis (Annexin V^+) was found in the INL and ONL only in the experimental group compared with the control group 48 hours after Aβ injection (indicated by white arrows in Fig. 2H). It was spatially consistent with the strong immunoreactivity of $A\beta_{1\text{-}40}$ found in a previous study.[10]

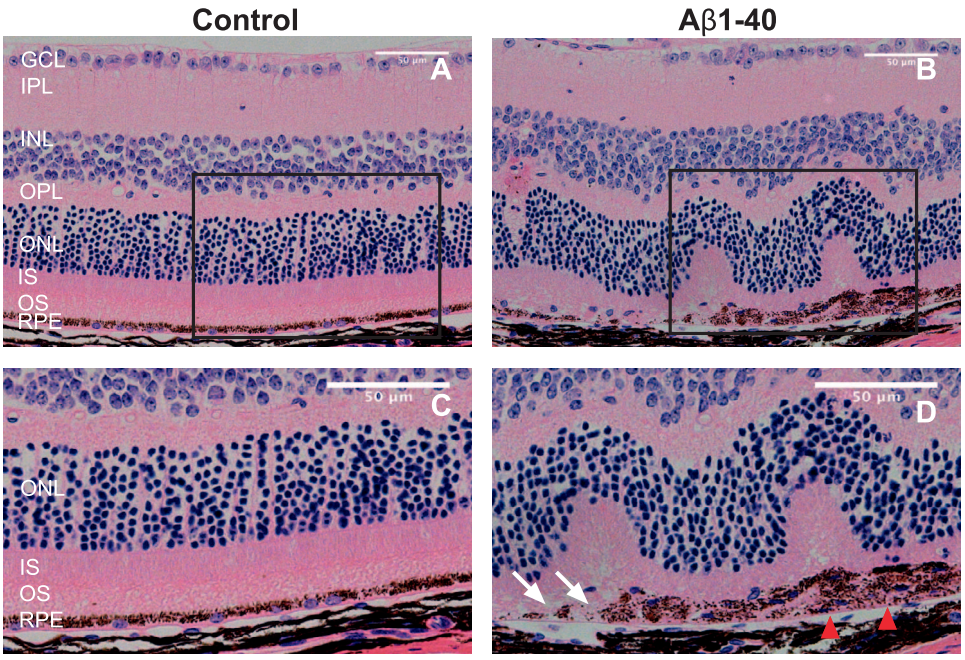

Figure 1. Aβ-induced morphologic changes of the retina. Hematoxylin and eosin (H&E)–stained paraffin sections of the retina and RPE layer from control mice (**A**) and $A\beta_{1\text{-}40}$-injected mice (**B**). (**C**, **D**) Magnified portions of images (**A**, **B**), respectively (enclosed in the *black boxes*). Disorganization of the outer retina and thinning of the IS/OS layer, especially the OS layer, were found. RPE changes such as hypopigmentation (*white arrows*), hyperpigmentation (*red triangles*), and irregular shapes were also found. GCL, ganglion cell layer; IPL, inner plexiform layer; INL, inner nuclear layer; OPL, outer plexiform layer; ONL, outer nuclear layer; IS, inner segment; OS, outer segment. *Scale bars*: 50 μm (**A**–**D**).

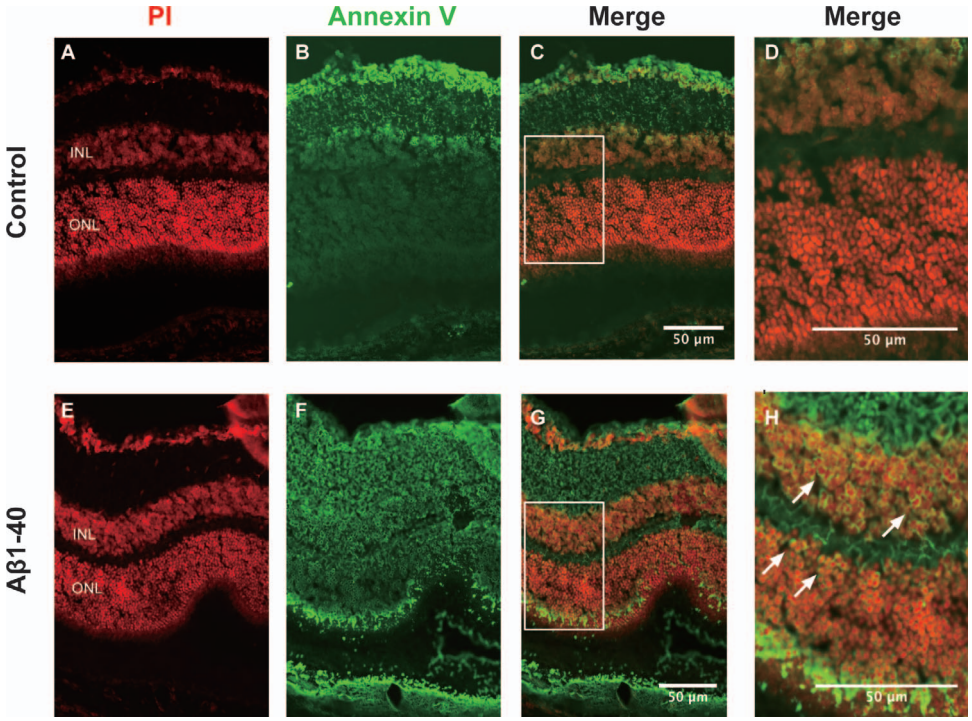

Figure 2. Aβ-induced apoptosis within the retina. Immunofluorescence assay via an Annexin V-FITC (*green*) and PI (*red*) staining method was employed to test apoptosis on day 2 in the control (**A**–**D**) and experimental groups (**E**–**H**). Images (**D**, **H**) are magnified portions of images (**C**, **G**), respectively (enclosed in the *white box*). Apoptosis (Annexin V^+) was found only in the ONL and INL in the experimental group compared with the control group 48 hours after Aβ injection (*white arrows*). *Scale bars*: 50 μm (**A**–**H**).

Investigative Ophthalmology & Visual Science

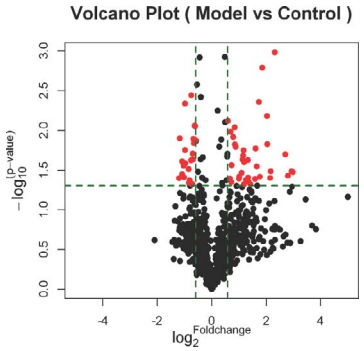

Figure 3. The volcano plots for the chip analysis. The diagram of the scatter plot demonstrates the differential expression between Aβ-injected mice and the PBS control groups. The *x*-axis is the mean value of $\log_2$-fold change, and the *y*-axis shows the $-\log_{10}$ of the *P* value. The *vertical green lines* represent the cutoff of 1.5-fold change up- or downregulated, and the *horizontal green line* represents the cutoff of *P* value significance ($P < 0.05$). In this manner, the *red points* represent the significantly differentially expressed miRNAs.

miRNA Profiling

The volcano plot (Fig. 3) aimed to visualize the significantly differentially expressed miRNAs (red point). The details of the significant data of the differentially expressed miRNAs on the chip can be found in Supplementary Figure S1.

Based on the cutoff at a fold change greater than 1.5 ($P < 0.05$), miRNA profiling revealed 61 differentially expressed miRNAs in all. Among these, 38 miRNAs were upregulated and 23 miRNAs were downregulated compared with the control group (Table 2).

RT-PCR Confirmation of the miRNA Microarray Results

To verify the chip results for the miRNAs of interest, RT-PCR was employed. According to the included criteria described in the Methods section, 10 miRNAs underwent confirmation, including the top 5 miRNAs that were overexpressed (miR-142, miR-1839, miR-216, miR-155, miR-223) and the top 5 miRNAs that were underexpressed (miR-744, miR-433, miR-1224, miR-200, miR-298). Finally, five miRNAs (miR-142, miR-216, miR-155, miR-223, and miR-433) were confirmed by qRT-PCR. However, the remaining five miRNAs showed nonsignificant differences (Fig. 4).

Functional Analysis of miRNAs and Target Gene Confirmation

Five miRNAs with the highest fold changes among the increased and decreased miRNAs were chosen for further bioinformatics analysis. We employed three databases to conduct the analyses to improve the accuracy of our predictions. In the miRanda, miRBase, and TargetScan databases, 11,968, 3886, and 1057 target genes were identified, respectively; 174 genes were common to the three databases and were subjected to further pathway analyses (Fig. 5).

Pathway analysis is a functional analysis mapping genes to KEGG pathways.[33] The *P* value (Fisher *P* value) denotes the significance of the pathway correlated with the conditions. The lower the *P* value, the more significant the pathway. The pathway analysis demonstrated the top 10 most related pathways and the targeted genes of the regulated miRNAs in Table 3. From the existing literature, we found that the ubiquitin-mediated proteolysis pathway (UPP) and the mitogen

Table 2. The miRNAs Displaying 1.5-Fold or More Change in Expression in Aβ-Injected Mice After 48 Hours as Determined by Microarray Analysis

ID	miRNAs Upregulated	Fold Change	*P* value
10947	mmu-miR-142a-3p	7.935	3.332E-02
146019	mmu-miR-1839-5p	7.578	3.247E-02
42511	mmu-miR-99a-3p*	6.940	3.721E-02
145707	mmu-miR-216b-5p	6.481	2.006E-02
27558	mmu-miR-155-5p	4.964	1.044E-03
42523	mmu-miR-26b-3p*	4.476	3.255E-02
42970	mmu-miR-744-3p*	4.405	3.957E-02
11024	mmu-miR-223-3p	4.110	1.485E-02
148242	mmu-miR-205-3p	4.072	6.585E-03
46774	mcmv-miR-m01-2-5p	3.606	1.632E-03
42636	mmu-miR-28a-3p	3.389	3.842E-02
148286	mmu-miR-3066-3p	3.303	4.385E-03
148608	mmu-miR-551b-5p	3.136	2.820E-02
145822	mmu-miR-214-5p	3.038	1.689E-02
42601	mmu-miR-540-5p	3.011	4.091E-02
148158	mghv-miR-M1-5-3p	2.661	4.781E-02
17624	mmu-miR-532-5p	2.542	4.432E-02
145859	mmu-miR-33-5p	2.525	3.901E-02
148051	mmu-miR-770-3p	2.510	2.353E-02
168787	mmu-miR-5114	2.385	4.225E-02
4700	mmu-miR-140-5p	2.275	2.493E-02
10955	mmu-miR-148a-3p	2.271	2.483E-02
28250	mmu-miR-872-5p	2.270	4.771E-02
42823	mmu-miR-27b-5p	2.249	1.775E-02
10952	mmu-miR-146a-5p	2.222	2.067E-02
168580	mmu-miR-5626-3p	2.189	2.315E-02
148655	mmu-miR-3471	2.137	3.396E-02
42804	mmu-miR-712-5p	2.012	3.799E-02
27855	mmu-miR-763	1.994	4.050E-02
42879	mmu-miR-92a-2-5p	1.839	1.592E-02
14313	mmu-miR-499-5p	1.800	1.501E-02
148578	mmu-miR-541-3p	1.792	9.107E-03
148099	mmu-miR-344h-3p	1.728	1.210E-02
42572	mmu-miR-154-3p	1.657	2.728E-02
146004	mmu-miR-2136	1.643	4.501E-02
14304	mmu-miR-376b-3p	1.614	1.036E-02
30973	mmu-miR-384-3p	1.592	4.051E-02
148476	mmu-miR-3552	1.512	7.610E-03

ID	miRNAs Downregulated	Fold Change	*P* Value
148450	mmu-miR-210-5p*	0.434	4.006E-02
27568	mmu-miR-744-5p	0.442	1.256E-02
168831	mmu-miR-433-3p	0.472	3.547E-02
46461	mmu-miR-1224-5p	0.472	2.433E-02
147186	mmu-miR-200b-3p	0.489	2.761E-02
147536	mmu-miR-107-5p*	0.493	3.896E-02
27572	mmu-miR-298-5p	0.506	4.589E-03
27533	mmu-miR-320-3p	0.508	1.761E-02
148333	mmu-miR-96-3p	0.511	2.583E-02
29190	mmu-miR-708-5p	0.554	3.051E-02
145638	mmu-miR-29a-5p	0.557	4.607E-02
28759	mmu-miR-758-3p	0.571	4.262E-02
28979	mmu-miR-670-5p	0.591	2.378E-02
145689	mmu-miR-543-3p	0.594	3.609E-03
42686	mmu-miR-136-3p	0.605	4.819E-02
11260	mmu-miR-151-5p	0.610	4.730E-02
148484	mmu-miR-3084-3p	0.618	1.953E-02
14301	mmu-miR-361-5p	0.618	2.324E-02
168966	mmu-miR-28a-5p/mmu-miR-28c	0.626	1.269E-02
168945	mmu-miR-326-3p	0.634	1.449E-02
17953	mmu-miR-183-3p	0.647	8.765E-03
148297	mmu-miR-92a-1-5p	0.655	8.832E-03
145634	mmu-miR-132-5p	0.661	1.327E-02

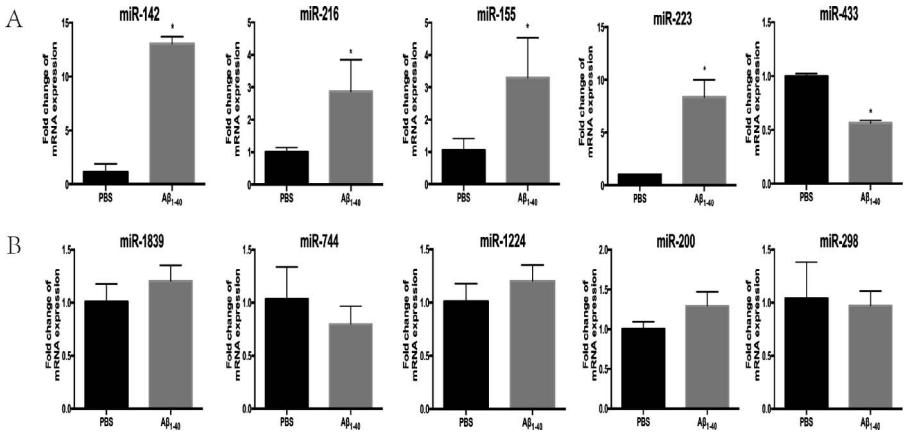

Figure 4. Confirmation of the differential expression of miRNAs in Aβ-induced retinal degeneration from PBS-injected controls using qRT-PCR. Values are expressed as fold change ± SEM compared with the control group. (**A**) miR-142, miR-216, miR-155, and miR-223 expression levels were upregulated and miR-433 expression levels were downregulated in the $A\beta_{1\text{-}40}$-injected group compared with controls. (**B**) miR-1839, miR-744, miR-1224, miR-200, and miR-298 expression levels remained nonsignificantly changed. $^*P < 0.05$; $n = 3$ per group. miRNA, microRNA; qRT-PCR, quantitative real-time PCR.

activated protein kinase (MAPK) signaling pathway had already been reported to be closely linked to partial AMD pathology.

After a literature review, several key downstream genes that are target genes of the confirmed miRNAs were examined by qRT-PCR (Fig. 6). Except for the level of *c-MET* expression in the neuroretina, the expression levels of *c-MET*, complement factor H (*CFH*), insulin-like growth factor 1 receptor (*IGF-1R*), and ATP-binding cassette transporter A1 (*ABCA1*) were the opposite of the expression levels of the corresponding miRNAs, consistent with the reported research on other tissues and experimental models.

Discussion

This is the first study to demonstrate the differentially expressed miRNA pattern in early AMD pathogenesis in an $A\beta_{1\text{-}40}$-induced retinal degeneration mouse model. In this study, we identified 38 upregulated and 23 downregulated miRNAs using a profiling microarray. In total, 5 of the 10 selected miRNAs and their target genes were identified as being differentially expressed by qRT-PCR. Kyoto Encyclopedia Genes and Genomes pathway analysis indicated the top 10 most related pathways in this Aβ-induced retinal degeneration model.

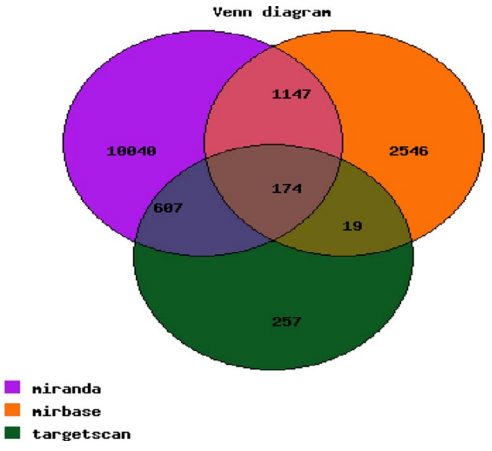

Figure 5. Venn diagram of the miRNA targets from the miRanda (*purple*), miRBase (*orange*), and TargetScan (*green*) databases.

Age-related macular degeneration is a multifactorial disease involving a range of complex genetic and environmental influences. Reflecting this complexity, there is currently no single animal model that develops all of the signs of AMD in a progressive manner, including ours.[34] Intravitreally injected Aβ is an acute retinal degeneration model rather than a progressive, gradual pathologic change like AMD. Nevertheless, our model has contributed to our understanding of how Aβ affects the miRNA profiling and target genes and their contribution to the etiology/pathogenesis of AMD.

In our preliminary experiment, we found that the levels of Aβ in the retina and RPE were most abundant on day 2, as were the levels of apoptosis and inflammation activation. This phenomenon is consistent with previous research and published studies.[10,35–37] Liu et al.[10] showed that the immunoreactivity of $A\beta_{1\text{-}40}$ undertaken with 4G8 revealed immunoreactivity in the neuropil and extracellular compartments throughout all retinal layers on day 1 and less on day 4. For the RPE, there were discrete intracellular vesicles possibly representing phagocytosed outer segment discs in the Aβ group compared with the reverse peptide group on day 1, while there were no vesicles on day 4. This time point is also consistent with Anderson's[35] and Walsh's[36] studies, which indicated that neural cell death occurred subsequent to the 48-hour window. In the study by Bruban et al.,[37] genes related to inflammation, oxidative stress, and apoptosis were mostly changed on day 3. In a study over a longer period of observation, Liu et al.[10] found that $A\beta_{1\text{-}40}$ could stimulate the upregulation of *IL-6* genes in the RPE/choroid and the neuroretina on day 1 and 4, but the changes became nonsignificant by later time points on days 14 and 49. Interleukin-6 is an inducer of acute-phase protein production, and its serum level has been associated with the progression of AMD, as has the prototypic cytokine TNF-a and proapoptotic gene *XAF1*. Therefore, we assumed that the changes in miRNA expression were probably significant by 2 days after the $A\beta_{1\text{-}40}$-induced retinal degeneration model based on the above evidence. In our further research, we will perform longer observations to confirm our assumptions.

For the selection of the drug supply, most similar experiments adopted intravitreal[10,35,38] or subretinal[15,39,40] injection of Aβ instead of intravenous injection. Intravitreal or subretinal injection can stimulate local pathogenesis to AMD more effectively than intravenous injection. In a study by Howlette et al.,[13] diffuse staining of Aβ across several layers of

Table 3. Top 10 Pathways of the 10 Most Dysregulated miRNA Targets

Pathway ID	Definition of the Pathway, *Mus musculus*, Mouse	Fisher *P* Value	Genes in Pathway
mmu05200	Pathways in cancer	0.0004	*COL4A4//CSF1R//CYCS//E2F3//FGF7//FGFR1//FZD5//GNB2//JUN//RELA//STK36//TCF7L2//TFG*
mmu04014	Ras signaling pathway	0.0009	*CSF1R//ELK1//FGF7//FGFR1//GNB2//PAK4//RELA//RGL2//RRAS*
mmu04810	Regulation of actin cytoskeleton	0.0027	*CFL2//FGF7//FGFR1//MYH10//PAK4//PXN//RRAS//WASL*
mmu04120	Ubiquitin-mediated proteolysis	0.0050	*CUL5//DET1//PPIL2//TRIM32//TRIP12//UBE2A*
mmu05161	Hepatitis B	0.0056	*CYCS//E2F3//ELK1//IKBKE//JUN//RELA*
mmu04010	MAPK signaling pathway	0.0069	*DUSP2//ELK1//FGF7//FGFR1//JUN//MAP3K11//RELA//RRAS*
mmu04932	Nonalcoholic fatty liver disease (NAFLD)	0.0079	*COX6B1//COX8A//CYCS//JUN//MAP3K11//RELA*
mmu05132	Salmonella infection	0.0109	*DYNC1I1//JUN//RELA//WASL*
mmu05222	Small cell lung cancer	0.0146	*COL4A4//CYCS//E2F3//RELA*

the retina extending as far as the outer plexiform layer was noted after intravitreal injection. Thus, there is no doubt that intravitreally injected Aβ can reach the whole of the retina and RPE/choroid layer and induce downstream changes. Therefore, this may be a useful mouse model with which to study local miRNA expression changes after Aβ stimulation.

Of note, the disorganization of the outer retina in the model group was more severe in our study compared to other similar studies.[10,15,35–42] Studies using Long-Evans rats[10] instead of C57BL/6 mice showed no morphologic changes or retinal cell apoptosis on retinal neurons in contrast to ours. Interestingly, in studies using Sprague-Dawley rats,[36,38] there were no morphologic changes, but retinal cell apoptosis appeared as early as day 2. We attributed the varied morphologic changes and apoptosis state mainly to the diverse Aβ responses between different species or strains. In the studies using C57BL/6,[15,37,39–42] the retina showed similar morphologic changes like disorganization of the photoreceptor nuclei and alteration of the inner segment (IS) and outer segment (OS) in the model group but these were still weaker than ours. Dinet et al.[40] reported that very few apoptotic photoreceptors observed by day 3 became numerous in the retinas on day 7. In our study, neuron apoptosis appeared on day 2. We attributed the differences to the different drug supply. In all these studies, the investigators conducted subretinal other than intravitreal injections with Aβ peptide, and well-organized neural retina tissues were analyzed a 300-μm distance from the center of the injection site to avoid confusion between the effects induced by the syringe itself and those induced by the injected Aβ.[15] The concentration of Aβ in the observation site was unavoidably decreased as it is 300 μm away from the injection site. As for our model, intravitreal injections were delivered and changes were observed on day 2, a time point at which the $A\beta_{1\text{-}40}$ levels were most abundant.[10] So the effect of Aβ on retina might be higher in our model. In conclusion, our model showed generally more severe changes of morphologic and retina cell apoptosis than the former studies, and we think this is mostly attributed to the different species and drug delivery methods.

Our chip results and subsequent confirmation runs provided insights into the miRNA dysregulation focused on dry AMD instead of on the wet type.[43–45] In our study, we found that Aβ could upregulate miR-155 levels in the retina. These observations were consistent with the findings in AMD retinas.[46] The previous authors found that the progressive, pathogenic increases in specific miR-155 could bind to the entire 232-nucleotide 3′-untranslated region (3′-UTR) of *CFH* and downregulate its expression. The deficiency of CFH could drive inflammatory neurodegeneration. In our study, we found for the first time that Aβ can induce the upregulation of miR-155, and the expression of *CFH* was correspondingly downregulated, implying a vital role of Aβ in complement system dysregulation by specific miRNA differential expression.

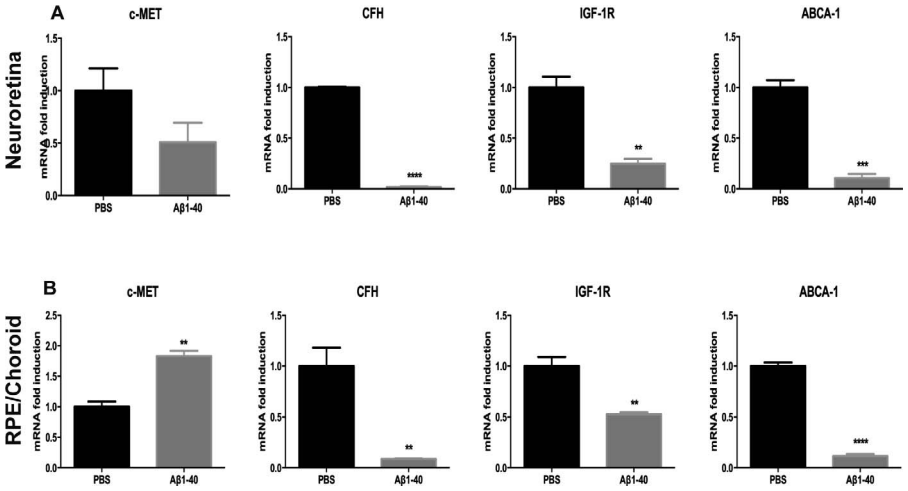

Figure 6. mRNA expression levels of downstream genes of selective miRNA RT-PCR data in Aβ-induced retinal degeneration and PBS-injected controls. Values are expressed as the fold change ± SEM relative to that of the control group. (**A**) Expression of *c-MET*, *CFH*, *IGF-1R*, and *ABCA1* in the neuroretina. (**B**) Expression levels of *c-MET*, *CFH*, *IGF-1R*, and *ABCA1* in the RPE/choroid, $^{*}P < 0.05$; $^{**}P < 0.01$, $^{***}P < 0.001$, $^{****}P < 0.001$; $n = 3$ per group. miRNA, microRNA; qRT-PCR, quantitative real-time PCR.

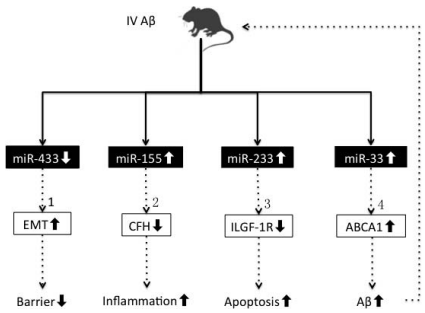

Figure 7. Schematic illustration of the changes induced by Aβ in the retina. After 48 hours, the levels of miR-155, miR-233, and miR-33 were upregulated and miR-433 was downregulated in response to $A\beta_{1\text{-}40}$ (represented by *solid lines*). The targeted genes of the miRNAs and their involved pathways (represented by *dashed lines*) were supported by the following studies: 1) Xu et al.[47]; 2) Lukiw et al.[46]; 3) Qadir et al.[48]; 4) Kim et al.[19] These target genes were confirmed in the neuroretina or RPE/choroid with same tendency in our study. IV, intravitreal injection.

It has been proven that Aβ can induce RPE barrier impairment.[7] In our study, we found one possible way for barrier dysregulation by Aβ through the downregulation of miR-433. Its downregulation could induce an epithelial–mesenchymal transition that impairs RPE barrier fuction.[47] Studies have also shown that miR-433 can activate c-MET/AKT/GSK-3β/Snail pathway, resulting in reduced cell–cell junctions. We also confirmed that the expression of *c-MET* is elevated in the RPE/choroid tissue. The RPE barrier functions as the outer barrier of the eyes. Our study indicated that overexpression of miR-433 might be a possible way to alleviate the impairment of the RPE barrier.

We found that the level of miR-233 increased after Aβ stimulation. Studies have reported that increasing miR-233 levels can induce apoptosis[48] and activate the unfolded protein response (UPR).[49] Specifically, miR-233 can target *IGF-1R*, which has a protective effect on Fas-induced hepatocyte apoptosis and liver injury. Although these studies were performed in other tissues, they have important implications in pathologic progress including apoptosis and UPR response in the retina. We subsequently confirmed the same effect of miR-233 on *IGF-1R* in the retina.

Aβ could induce the upregulation of miR-33 in our study (Supplementary Fig. S1). It has been clearly reported that miR-33 regulates ABCA1 and Aβ levels in the brain.[19] MicroR-33 could reduce the expression of the *ABCA1* gene by binding to the 3′UTR of *ABCA1*. ABCA1 has a positive effect on ApoE lipidation and an inhibitory effect on Aβ levels. This phenomenon implied a possible feedback mechanism for Aβ accumulation in RPE cells. Most importantly, inhibition of miR-33 might decrease Aβ levels in the retina, representing a potential therapeutic strategy for AMD. The possible role of all confirmed regulated miRNAs and their important functions related to AMD pathologies are summarized in Figure 7.

There were five miRNAs identified by the microarray that showed nonsignificant changes by PCR. We attributed the difference to the different sampling and processing methods between the chip screening and poly(A) tail–based RT-PCR assays. Chip results are obtained in a high-throughput manner through RNA labeling and hybridization on miRNA microarray chips, and it provides initial experimental directions; thus, chip screening is usually applied at the screening stage. However, chip screening has unavoidable innate disadvantages such as a high false-positive rate. Therefore, we used poly(A) tail–based RT-PCR assays to avoid the false-positive targets. In this way, the consistent results confirmed both by chip hybridization and by poly(A) tail–based RT-PCR are more reliable.

Pathway analyses indicated that the miRNA target genes might be primarily involved in the ubiquitin-mediated proteolysis and the MAPK signaling pathways based on our chip results. These two pathways play important roles in AMD pathogenesis. Proper function of the UPP is crucial for protein-selective degradation. In contrast, age- or stress-induced impairment of UPP function may lead to the accumulation of abnormal proteins, such as drusen, in the retina.[50] In addition, oxidative stress is considered to be a very important factor in dry AMD that can activate downstream pathways, including the MAPK pathway.[51]

Interestingly, although the inflammatory pathway was not implicated in informatics analyses, genes in the pathway such as *RELA*, *CSF1R*, *IKBKE*, and *RRAS* all appeared in the predictions (Table 3). Chronic inflammation caused by Aβ has been widely reported.[52] RelA is a subunit of nuclear factor-kappa B (NF-κB), a key regulator of the inflammation response.[53] The IκB kinase inhibitor of κB kinase epsilon (IKBKE) is an IκB kinase family member that can also activate the AKT and NF-κB pathways; IKBKE is also involved in the interleukin-1 (IL-1) signaling pathway. Our prior study confirmed that IL-1b could mediate RPE inflammation in an A2E-induced cell model.[54] Colony-stimulating factor-1 receptor (CSF-1R) plays an important role in innate immunity and in inflammatory processes in which CSF-1 and interleukin-34 (IL-34) compete for binding. Recent studies[55] have revealed that CSF-1R signaling directly controls retinal microglia inflammation and might play a relevant role in neurodegenerative diseases such as AMD.

Cancer in pathways ranked first in the informatics prediction. This result might be attributable to common pathways shared with Aβ-induced changes such as apoptosis, angiogenesis, vascular homeostasis, regeneration, cell adhesion, and neuronal axon guidance. Some pathways, such as hepatitis B and salmonella infection, seemed not to be correlated with our model at first glance. We propose that they were suggested for several possible reasons. First, certain similar miRNA changes are shared after hepatitis B (HBV) or salmonella infection and in our model. As reported, miR-27b-5p[56] and miR-23b-3p[57,58] were upregulated after HBV infection, and miR-26b,[59] mir-532-5p,[60] and mir-27b[60] were upregulated after salmonella infection. These miRNAs show the same tendency of changes after Aβ stimulation. Secondly, during HBV infection, the host genome integrates the HBV DNA and produces viral proteins such as HBx, hepatitis B surface antigen (HBsAg), and HBeAg. These viral proteins can trigger cancer-related genes and motivate several signaling pathways including genetic instability, inflammatory, and host immune responses.[56] These pathways, especially the proliferation[57,61–63] and apoptosis[58,63] pathways, were included in our model. Thirdly, as we made predictions with limited confirmed miRNA data, some possible pathways might be missing as an inevitable undesired result. This is also a limitation of our study.

Our data partially explain the dysregulation of miRNAs induced by $A\beta_{1\text{-}40}$ and how the drusen component Aβ affected the retina by regulating miRNAs. Furthermore, the confirmed up- or downregulated miRNAs might act as therapeutic targets, but this possibility requires further confirmation. MicroRNA regulation was deemed to be species specific. Hence, great caution should be exercised when the results obtained from mice are translated to human disease. Nevertheless, our preliminary results are valuable, as they indicate several directions with great promise.

In summary, our results provide the first foundation for global miRNA expression pattern analysis in Aβ-related retinal

degeneration to provide novel therapeutic targets for diseases such as AMD. We identified 61 miRNAs that were differentially expressed between the Aβ-injected and the control groups, including 38 upregulated and 23 downregulated miRNAs. The confirmed miRNAs showed great functional roles in biochemistry processes such as complement activation, barrier impairment, apoptosis, and positive feedback for Aβ accumulation. According to the KEGG pathway analyses, we found that the target genes were primarily involved in ubiquitin-mediated proteolysis and the MAPK signaling pathways in this model, which play important roles in the initiation and progression of dry AMD. Although inflammatory pathways were not listed, several important preinflammatory factors or regulators were also suggested. Because miRNAs are endogenous molecules with a very low nonspecific immune response,[64] balancing abnormal miRNA expression levels might be a relatively safe way to alleviate the detrimental effects of drusen deposits of Aβ on the retina.

Acknowledgments

Supported by the National Natural Science Foundation of China (Grant 81425006), Shanghai Creative Key Medical Research Grant (1341195400), Translational Medicine Grant of Shanghai Jiao Tong University, School of Medicine (5ZH4005), Shanghai Engineering Center for Visual Science and Photomedicine Science (16dz2251500), and Technology Commission of Shanghai Municipality (16140900800).

Disclosure: **P. Huang**, None; **J. Sun**, None; **F. Wang**, None; **X. Luo**, None; **J. Feng**, None; **Q. Gu**, None; **T. Liu**, None; **X. Sun**, None

References

1. Klein R, Peto T, Bird A, Vannewkirk MR. The epidemiology of age-related macular degeneration. *Am J Ophthalmol*. 2004; 137:486–495.
2. Congdon N, O'Colmain B, Klaver CC, et al. Causes and prevalence of visual impairment among adults in the United States. *Arch Ophthalmol*. 2004;122:477–485.
3. Rosenfeld PJ, Brown DM, Heier JS, et al. Ranibizumab for neovascular age-related macular degeneration. *N Engl J Med*. 2006;355:1419–1431.
4. Hogg RE, Stevenson MR, Chakravarthy U, Beirne RO, Anderson RS. Early features of AMD. *Ophthalmology*. 2007; 114:1028.
5. Isas JM, Luibl V, Johnson LV, et al. Soluble and mature amyloid fibrils in drusen deposits. *Invest Ophthalmol Vis Sci*. 2010;51: 1304–1310.
6. Yoshida T, Ohno-Matsui K, Ichinose S, et al. The potential role of amyloid beta in the pathogenesis of age-related macular degeneration. *J Clin Invest*. 2005;115:2793–2800.
7. Park SW, Kim JH, Mook-Jung I, et al. Intracellular amyloid beta alters the tight junction of retinal pigment epithelium in 5XFAD mice. *Neurobiol Aging*. 2014;35:2013–2020.
8. Hoh Kam J, Lynch A, Begum R, Cunea A, Jeffery G. Topical cyclodextrin reduces amyloid beta and inflammation improving retinal function in ageing mice. *Exp Eye Res*. 2015;135: 59–66.
9. Ding JD, Johnson LV, Herrmann R, et al. Anti-amyloid therapy protects against retinal pigmented epithelium damage and vision loss in a model of age-related macular degeneration. *Proc Natl Acad Sci U S A*. 2011;108:E279–E287.
10. Liu RT, Gao JY, Cao SJ, et al. Inflammatory mediators induced by amyloid-beta in the retina and RPE in vivo: implications for inflammasome activation in age-related macular degeneration. *Invest Ophthalmol Vis Sci*. 2013;54:2225–2237.
11. Prakasam A, Anusuyadevi M, Ablonczy Z, et al. Differential accumulation of secreted A betaPP metabolites in ocular fluids. *J Alzheimers Dis*. 2010;20:1243–1253.
12. Kurji KH, Cui JZ, Lin T, et al. Microarray analysis identifies changes in inflammatory gene expression in response to amyloid-beta stimulation of cultured human retinal pigment epithelial cells. *Invest Ophthalmol Vis Sci*. 2010;51:1151–1163.
13. Howlett DR, Bate ST, Collier S, et al. Characterisation of amyloid-induced inflammatory responses in the rat retina. *Exp Brain Res*. 2011;214:185–197.
14. Cao LN, Wang H, Wang F, Xu D, Liu F, Liu CQ. Aβ-induced senescent retinal pigment epithelial cells create a proinflammatory microenvironment in AMD. *Invest Ophthalmol Vis Sci*. 2013;54:3738–3750.
15. Bruban J, Glotin AL, Dinet V, et al. Amyloid-beta(1-42) alters structure and function of retinal pigmented epithelial cells. *Aging Cell*. 2009;8:162–177.
16. Parsons CG, Ruitenberg M, Freitag CE, Sroka-Saidi K, Russ H, Rammes G. MRZ-99030 - a novel modulator of Aβ aggregation: I - mechanism of action (MoA) underlying the potential neuroprotective treatment of Alzheimer's disease, glaucoma and age-related macular degeneration (AMD). *Neuropharmacology*. 2015;92:158–169.
17. Koyama Y, Matsuzaki S, Gomi F, et al. Induction of amyloid beta accumulation by ER calcium disruption and resultant upregulation of angiogenic factors in ARPE19 cells. *Invest Ophthalmol Vis Sci*. 2008;49:2376–2383.
18. Chen L, Bai Y, Zhao M, Jiang Y. TLR4 inhibitor attenuates amyloid-beta-induced angiogenic and inflammatory factors in ARPE-19 cells: implications for age-related macular degeneration. *Mol Med Rep*. 2016;13:3249–3256.
19. Kim J, Yoon H, Horie T, et al. microRNA-33 regulates ApoE lipidation and amyloid-beta metabolism in the brain. *J Neurosci*. 2015;35:14717–14726.
20. Soifer HS, Rossi JJ, Saetrom P. MicroRNAs in disease and potential therapeutic applications. *Mol Ther*. 2007;15:2070–2079.
21. Huntzinger E, Izaurralde E. Gene silencing by microRNAs: contributions of translational repression and mRNA decay. *Nat Rev Genet*. 2011;12:99–110.
22. Krol J, Busskamp V, Markiewicz I, et al. Characterizing light-regulated retinal microRNAs reveals rapid turnover as a common property of neuronal microRNAs. *Cell*. 2010;141: 618–631.
23. Grassmann F, Schoenberger PG, Brandl C, et al. A circulating microrna profile is associated with late-stage neovascular age-related macular degeneration. *PLoS One*. 2014;9:e107461.
24. Zhou Q, Anderson C, Zhang H, et al. Repression of choroidal neovascularization through actin cytoskeleton pathways by microRNA-24. *Mol Ther*. 2014;22:378–389.
25. Kaneko H, Dridi S, Tarallo V, et al. DICER1 deficit induces Alu RNA toxicity in age-related macular degeneration. *Nature*. 2011;471:325–330.
26. Bloomston M, Frankel WL, Petrocca F, et al. MicroRNA expression patterns to differentiate pancreatic adenocarcinoma from normal pancreas and chronic pancreatitis. *JAMA*. 2007;297:1901–1908.
27. Xing S, Shen D, Chen C, Wang J, Liu T, Yu Z. Regulation of neuronal toxicity of beta-amyloid oligomers by surface ATP synthase. *Mol Med Rep*. 2013;8:1689–1694.
28. Yan Q, Zhu H, Wang FH, et al. Inhibition of TRB3 protects photoreceptors against endoplasmic reticulum stress-induced apoptosis after experimental retinal detachment. *Curr Eye Res*. 2016;41:240–248.
29. Wang W, Wang F, Lu F, et al. The antiangiogenic effects of integrin alpha5beta1 inhibitor (ATN-161) in vitro and in vivo. *Invest Ophthalmol Vis Sci*. 2011;52:7213–7220.

30. Guo L, Normando EM, Nizari S, Lara D, Cordeiro MF. Tracking longitudinal retinal changes in experimental ocular hypertension using the cSLO and spectral domain-OCT. *Invest Ophthalmol Vis Sci*. 2010;51:6504–6513.
31. Liu T, Cheng W, Gao Y, Wang H, Liu Z. Microarray analysis of microRNA expression patterns in the semen of infertile men with semen abnormalities. *Mol Med Rep*. 2012;6:535–542.
32. Feng J, Chen X, Sun X, Wang F, Sun X. Expression of endoplasmic reticulum stress markers GRP78 and CHOP induced by oxidative stress in blue light-mediated damage of A2E-containing retinal pigment epithelium cells. *Ophthalmic Res*. 2014;52:224–233.
33. Xu N, Wang F, Lv M, Cheng L. Microarray expression profile analysis of long non-coding RNAs in human breast cancer: a study of Chinese women. *Biomed Pharmacother*. 2015;69:221–227.
34. Dilks DD, Julian JB, Peli E, Kanwisher N. Reorganization of visual processing in age-related macular degeneration depends on foveal loss. *Optom Vis Sci*. 2014;91:e199–e206.
35. Anderson PJ, Watts H, Hille C, et al. Glial and endothelial blood-retinal barrier responses to amyloid-beta in the neural retina of the rat. *Clin Ophthalmol*. 2008;2:801–816.
36. Walsh DT, Montero RM, Bresciani LG, et al. Amyloid-beta peptide is toxic to neurons in vivo via indirect mechanisms. *Neurobiol Dis*. 2002;10:20–27.
37. Bruban J, Maoui A, Chalour N, et al. CCR2/CCL2-mediated inflammation protects photoreceptor cells from amyloid-beta-induced apoptosis. *Neurobiol Dis*. 2011;42:55–72.
38. Walsh DT, Bresciani L, Saunders D, et al. Amyloid beta peptide causes chronic glial cell activation and neuro-degeneration after intravitreal injection. *Neuropathol Appl Neurobiol*. 2005;31:491–502.
39. Liu C, Cao L, Yang S, et al. Subretinal injection of amyloid-beta peptide accelerates RPE cell senescence and retinal degeneration. *Int J Mol Med*. 2015;35:169–176.
40. Dinet V, Bruban J, Chalour N, et al. Distinct effects of inflammation on gliosis, osmohomeostasis, and vascular integrity during amyloid beta-induced retinal degeneration. *Aging Cell*. 2012;11:683–693.
41. Park SW, Kim JH, Park SM, et al. RAGE mediated intracellular Aβ uptake contributes to the breakdown of tight junction in retinal pigment epithelium. *Oncotarget*. 2015;6:35263–35273.
42. Taylor-Walker G, Lynn SA, Keeling E, et al. The Alzheimer's-related amyloid beta peptide is internalised by R28 neuroretinal cells and disrupts the microtubule associated protein 2 (MAP-2). *Exp Eye Res*. 2016;153:110–121.
43. Shen J, Yang X, Xie B, et al. MicroRNAs regulate ocular neovascularization. *Mol Ther*. 2008;16:1208–1216.
44. Zhou Q, Gallagher R, Ufret-Vincenty R, Li X, Olson EN, Wang S. Regulation of angiogenesis and choroidal neovascularization by members of microRNA-23∼27∼24 clusters. *Proc Natl Acad Sci U S A*. 2011;108:8287–8292.
45. Lin H, Qian J, Castillo AC, et al. Effect of miR-23 on oxidant-induced injury in human retinal pigment epithelial cells. *Invest Ophthalmol Vis Sci*. 2011;52:6308–6314.
46. Lukiw WJ, Surjyadipta B, Dua P, Alexandrov PN. Common micro RNAs (miRNAs) target complement factor H (CFH) regulation in Alzheimer's disease (AD) and in age-related macular degeneration (AMD). *Int J Biochem Mol Biol*. 2012;3:105–116.
47. Xu X, Zhu Y, Liang Z, et al. c-Met and CREB1 are involved in miR-433-mediated inhibition of the epithelial-mesenchymal transition in bladder cancer by regulating Akt/GSK-3beta/Snail signaling. *Cell Death Dis*. 2016;7:e2088.
48. Qadir XV, Chen W, Han C, Song K, Zhang J, Wu T. miR-223 deficiency protects against Fas-induced hepatocyte apoptosis and liver injury through targeting insulin-like growth factor 1 receptor. *Am J Pathol*. 2015;185:3141–3151.
49. Dai LL, Gao JX, Zou CG, Ma YC, Zhang KQ. mir-233 modulates the unfolded protein response in *C. elegans* during *Pseudomonas aeruginosa* infection. *PLoS Pathogens*. 2015;11:e1004606.
50. Shang F, Taylor A. Roles for the ubiquitin-proteasome pathway in protein quality control and signaling in the retina: implications in the pathogenesis of age-related macular degeneration. *Mol Aspects Med*. 2012;33:446–466.
51. Koinzer S, Reinecke K, Herdegen T, Roider J, Klettner A. Oxidative stress induces biphasic ERK1/2 activation in the RPE with distinct effects on cell survival at early and late activation. *Curr Eye Res*. 2015;40:853–857.
52. Cao L, Liu C, Wang F, Wang H. SIRT1 negatively regulates amyloid-beta-induced inflammation via the NF-kappaB pathway. *Braz J Med Biol Res*. 2013;46:659–669.
53. Chen L, Fischle W, Verdin E, Greene WC. Duration of nuclear NF-kappaB action regulated by reversible acetylation. *Science*. 2001;293:1653–1657.
54. Shi Q, Wang Q, Li J, et al. A2E Suppresses regulatory function of RPE cells in Th1 cell differentiation via production of IL-1beta and inhibition of PGE2. *Invest Ophthalmol Vis Sci*. 2015;56:7728–7738.
55. Liu W, Xu GZ, Jiang CH, Tian J. Macrophage colony-stimulating factor and its receptor signaling augment glycated albumin-induced retinal microglial inflammation in vitro. *BMC Cell Biol*. 2011;12:5.
56. Jinato T, Chuaypen N, Poomipak W, et al. Original research: analysis of hepatic microRNA alterations in response to hepatitis B virus infection and pegylated interferon alpha-2a treatment. *Exp Biol Med (Maywood)*. 2016;241:1803–1810.
57. Rogler CE, Levoci L, Ader T, et al. MicroRNA-23b cluster microRNAs regulate transforming growth factor-beta/bone morphogenetic protein signaling and liver stem cell differentiation by targeting Smads. *Hepatology*. 2009;50:575–584.
58. Yuan B, Dong R, Shi D, et al. Down-regulation of miR-23b may contribute to activation of the TGF-beta1/Smad3 signalling pathway during the termination stage of liver regeneration. *FEBS Lett*. 2011;585:927–934.
59. Yao M, Gao W, Tao H, Yang J, Liu G, Huang T. Regulation signature of miR-143 and miR-26 in porcine Salmonella infection identified by binding site enrichment analysis. *Mol Genet Genomics*. 2016;291:789–799.
60. Bao H, Kommadath A, Liang G, et al. Genome-wide whole blood microRNAome and transcriptome analyses reveal miRNA-mRNA regulated host response to foodborne pathogen Salmonella infection in swine. *Sci Rep*. 2015;5:12620.
61. Zhang Q, Yuan Y, Cui J, Xiao T, Jiang D. MiR-217 promotes tumor proliferation in breast cancer via targeting DACH1. *J Cancer*. 2015;6:184–191.
62. Zhao WG, Yu SN, Lu ZH, Ma YH, Gu YM, Chen J. The miR-217 microRNA functions as a potential tumor suppressor in pancreatic ductal adenocarcinoma by targeting KRAS. *Carcinogenesis*. 2010;31:1726–1733.
63. Chen B, Duan L, Yin G, Tan J, Jiang X. Simultaneously expressed miR-424 and miR-381 synergistically suppress the proliferation and survival of renal cancer cells—Cdc2 activity is up-regulated by targeting WEE1. *Clinics (Sao Paulo)*. 2013;68:825–833.
64. Saxena K, Rutar MV, Provis JM, Natoli RC. Identification of miRNAs in a model of retinal degenerations. *Invest Ophthalmol Vis Sci*. 2015;56:1820–1829.

Investigative Ophthalmology & Visual Science